ORIGINAL PAPER

Wedge failure hazard assessment by means of a probabilistic approach for an unstable sea-cliff

Paolo Budetta · Claudio De Luca

Abstract   This paper deals with a probabilistic approach for the slope safety factor calculation that uses kinematic and kinetic instability assessment of wedge failures affecting an unstable sea-cliff. The cliff, located at Agropoli (province of Salerno, Campania) along a coastal stretch of Southern Italy, is about 240 m long with height ranging between 10 and 55 m. Detailed geological, geo-structural and geo-mechanical surveys were performed in situ, whereas joint and rock strength parameters were measured in the laboratory. Wedge failures are the most frequent episodic phenomena favoured by the geo-structural and geo-mechanical layout of the rock mass, and subordinately the assailing force of waves. Based on the orientation of the discontinuities, with respect to the cliff face, the main joint set intersections which may cause potential unstable wedges have been identified. As during heavy sea storms, wave energy may contribute to cliff instability, and also an in-depth study regarding wave characteristics and direction affecting the coastal stretch where the sea-cliff is located was performed. The probabilistic stability analysis, performed using the SWEDGE software, allowed the identification of joint set intersections with high wedge failure probabilities. The failure probability is strongly affected by the geo-structural and geo-mechanical layout of the rock mass. In this respect, the random properties of orientation of joints which define the wedges and their shear strength have an important effect in the safety factor calculation. As the deterministic approach does not take into account the variability of these parameters and can provide simplified and misleading results, the simultaneous analysis of kinematic and kinetic conditions can provide a better evaluation of the overall stability. Finally, a wedge probability failure zonation of the whole sea-cliff was proposed.

Keywords   Sea-cliff · Wedge failure · Geo-mechanical characterization · Probabilistic landslide analysis

P. Budetta (✉) · C. De Luca
Department of Civil, Architectural and Environmental Engineering, University of Naples "Federico II", Piazzale Tecchio, 80, 80125 Naples, Italy
e-mail: paolo.budetta@unina.it

1 Introduction

It is estimated that more than 41 % of the regional population lives along the Campania shoreline of the Southern Italy and that more than 53 % of this coast is rocky. Wedge failures, topples and translational slides from sea-cliffs are among the main threats affecting infrastructures and residential areas located along the coast. These landslides commonly involve small volumes, but they affect areas with high-density occupation by people and buildings, thus significantly increasing risk conditions (Di Crescenzo and Santo 2007; Budetta et al. 2008).

In the last 2,000 years, in tectonically stable areas of the Mediterranean Sea, the sea level has risen about 1.30 m (Antonioli and Silenzi 2007), and it is predictable that, in 2100, a further rise in the sea level, varying between 0.09 and 0.30 m, can be expected (Church and White 2006; IPCC 2007). As a result, due to the decreased dissipative effect with regard to the wave energy affecting submerging shore platforms, a marked rise in the coastal erosion of rocky coasts will also happen. In fact, shore platforms tend to assume an equilibrium profile able to dissipate the energy of waves during heavy sea storms. Their quick sinking, in addition to the rapid removal of coarse debris at cliff toes, will cause an increase in the cliff retreat rate (Dubois 2002; Ashton et al. 2011).

The basic factors controlling sea-cliff instability are well known: the force of waves as well as the strength of exposed rock masses. Additional factors are reduction in rock strength owing to weathering by sea spray, tidal action, heavy rainfalls and material fatigue caused by cyclic loading of waves (Sunamura 1992). Due to many variables involved, the transfer of the wave energy to the cliff, which is able to produce instability, is still a mechanism hard to quantify. In fact, it is difficult to quantify: (1) the deep-water wave climate (2) how the deep-water energies of waves are modified by sea floor before they reach the coast, (3) the dissipation of wave energy by breaking in the near shore and (4) the dynamic pressure of waves at cliff base. For sea-cliffs affecting long coastal stretches, several papers have been proposed in order to estimate the landslide hazard from a point of view of interactions between wave energy, erosion rate and strength of exposed rock masses (Budetta et al. 2000; Trenhaile 2002; Kogure et al. 2006; Hall et al. 2008; Naylor and Stephenson 2010; De Vita et al. 2012; Castedo et al. 2013; Marques et al. 2013). These studies take into account a set of predisposing factors, such as the wave characteristics, erosion rates, lithological layout and historical or present instability. Then, the relative hazard is usually evaluated on the basis of qualitative (geomorphological mapping, heuristic approaches, etc.) or quantitative (bivariate or multivariate statistical analyses, deterministic approaches, etc.) methods.

On the contrary, where retreat velocities affecting short cliffs carved in competent rocks are low, difficulties in monitoring erosion processes can hamper the hazard assessment. Furthermore, although it is tempting to ascribe the formation of coastal cliffs entirely to marine erosional processes, sometimes other natural or human causes can be equally important. The shape of a coastal cliff, in particular its steepness, is generally related to the interplay of marine and gravitative processes acting on outcropping rock masses with different strength, and it is impossible to assign well-defined percentage weights to both these triggering factors. Cliff collapses can be episodic and discontinuous in time and space, and occur where rock masses are very fractured in response to single large sea storms (Andriani and Walsh 2007; Paronuzzi 2010; Budetta 2011; Martino and Mazzanti 2013). In such cases, no quantitative model has yet been proposed for evaluating the action of the assailing force of waves on the kinetic evolution of rock failures (Castedo et al. 2013). Consequently, multidisciplinary approaches designed to integrate geologic and geomorphic field mapping, topographical surveys and marine numerical dating techniques in a quantitative hazard analysis are hard to perform.

In this paper, regarding a restricted area, where several of the above-mentioned impediments are present, we applied a geo-mechanical probabilistic approach based on the kinematic and kinetic instability assessment of possible wedge failures. These landslides are caused by the unfavourable geo-structural and geo-mechanical layout of the rock mass and, to a lesser extent, the assailing force of waves. With reference to this last matter, an in-depth study regarding the wave energy and direction affecting the physiographic unit where the study area is located was performed. The ultimate goal of the research is to identify and map sea-cliff sectors with high wedge failure probabilities. In the past, the area has been already affected by wedge failures, and only for a few of these events, triggering dates and volumes are known. Furthermore, there are no available maps to show, in time, the evolution of the whole slope face and to calculate erosion rate. The study is also based on a detailed photogrammetric survey, geo-structural investigations, boreholes, water pressure and laboratory tests.

2 The studied cliff and its geo-structural layout

The studied sea-cliff is located at Agropoli (Cilento, province of Salerno) along a coastal stretch of Southern Italy and extends itself for about 240 m (Fig. 1). The slope belongs to a
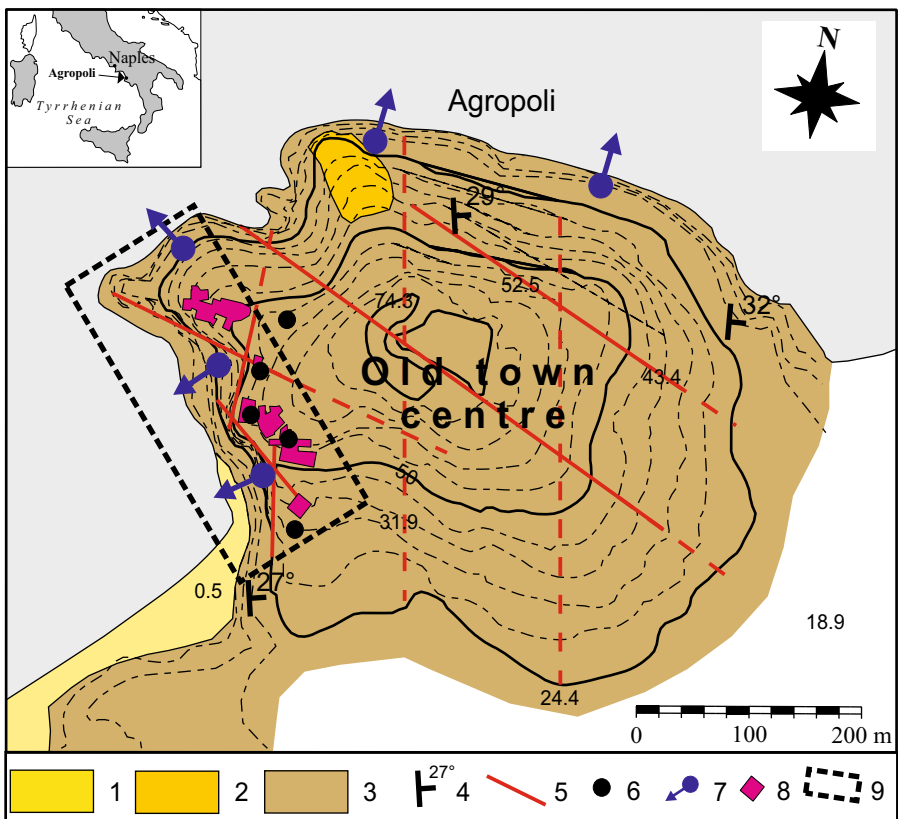

Fig. 1 Geological map of the Agropoli promontory. 1 Present beaches; 2 ancient cemented marine sands; 3 marls and calcareous marls; 4 attitude of bedding planes; 5 main fault (presumed if it is a *dashed line*); 6 borehole; 7 landslide; 8 building exposed to landslide hazard; 9 the studied area

wide promontory on which the old town centre is located. Due to unstable slope conditions, some buildings located on the hill top, as well as a sandy beach at the cliff base exploited for bathing purposes, are exposed to high-risk conditions. Over the last 30 years, several wedge failures occurred along the entire headland, and particularly along the studied cliff.

By means of a photogrammetric survey, the cliff geometry has been carefully evaluated. The photogrammetric survey (original scale 1/200) was based on photographs collected from the sea. Then, using a total station, digital data were adjusted and transformed to local x–y–z coordinates. Original contour lines, representing in great detail the shape of the cliff face, are characterized by a spacing of 0.20 m and are related to an ideal vertical reference plan located backwards the cliff. To ensure a more clear representation, and use this photogrammetric survey as a base map for the wedge failure probability zonation, a simplified version of the map is shown (see Fig. 1).

The sea-cliff height ranges between 10 and 55 m with a mean value of about 35 m. A predominant steep, sharp-crested and unvegetated profile with sparse debris at the slope base indicates a retreating coastal cliff due to undercutting by waves and gravitative processes. The slope face (dipping on average 80°) was generated by the intersections of large fault scarps (NW–SE and NE–SW oriented), caused by tectonic uplifting during the Pliocene and the lower Pleistocene (Bonardi et al. 2009). Consequently, in a contour plan, it shows a tortuous pattern characterized by sudden orientation changes (Fig. 1). Other high-persistent discontinuities affect the outcropping rock mass that appears heavily fractured. Joint intersections with different orientations isolate potential wedges with variable volumes. On the cliff face, calcareous marls crop out that gently dip to the NE. These rocks, belonging to the "San Mauro" Formation, consist of Langhian-Upper Burdigalian grey-to-bluish-grey calcareous marly strata. They are important key horizons, known as "Fogliarine del Cilento", occurring at different stratigraphic heights between conglomeratic-arenaceous strata of the "San Mauro" Formation (Bonardi et al. 2009; Budetta and Nappi 2011).

According to the suggested methods by ISRM (2007) and Palmström (2005), the quantitative and qualitative description of about 260 discontinuities (orientation, spacing,
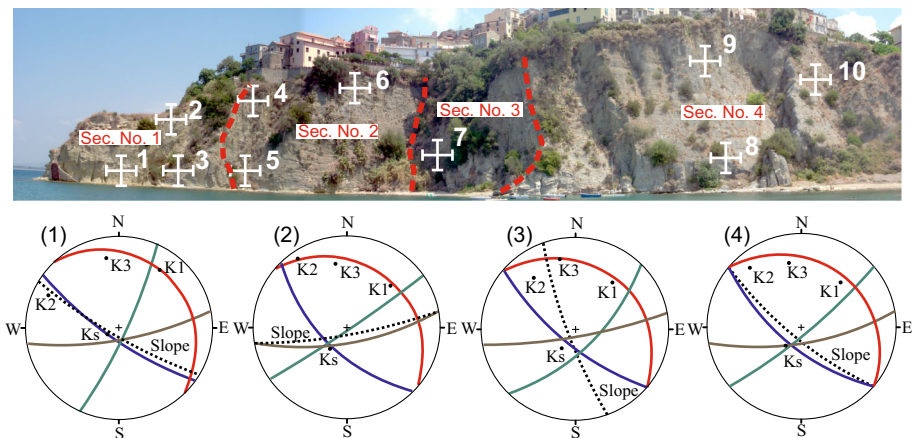

Fig. 2 Wide shot showing the studied sea-cliff and the identified homogeneous geo-structural sectors. The *white crosses* locate the geo-structural stations. Stereographic projections of the joint sets affecting the four sectors

persistence, aperture, infilling materials and roughness of joint surfaces) has been carefully performed by experienced rock-climber geologists. Given the difficult accessibility to the sea-cliff, geo-structural data were surveyed in ten stations, and the whole slope was sub-divided in four homogeneous geo-structural sectors characterized by different cliff face and joint set orientations (Fig. 2). The joint orientation data were statistically processed to determine their mean value (M), standard deviation (σ) and coefficient of variation (C_v) and plotted on the equal area stereographic projection representing the mean orientation of the main discontinuity sets affecting the sea-cliff (Fig. 3). The stereonet highlights the presence of 4 joint sets which group the bedding planes (Ks) as well as tectonic discontinuities (K1, K2 and K3) with different mean orientations. Even though discontinuities belonging to the joint set K1 show a high-orientation scattering (which might suggest splitting it into two subsets), for the sake of simplicity, in the following stability analysis (see Fig. 3), a single joint system was considered (Fig. 3). The above-mentioned wedges appear caused by intersections between sets K1–K2 and K1–K3. With respect to the mean cliff face orientation, these wedges show mean intersection lines with orientations (trend/plunge) of 185°/45° and 240°/60°. In this regard, it is important to point out that the variations of the cliff face direction, with reference to local joint orientations surveyed in the four geo-structural sectors, may affect the kinematic effectiveness of some of the joint intersections to allow wedge failures (Fig. 2).

From processing of field data, the following conclusions can be inferred. The joint set Ks shows medium persistence (5–7 m), and its spacing generally ranges between 210 and 250 mm ("moderate" spacing). The bedding planes dip into the rock face favouring a better stability. With reference to the other sets, spacing values generally vary between "very close" to "wide" with a mean value of 61 mm ("close" spacing).

Regarding the other physical properties of joints, it can be observed that:

- The joint surfaces present themselves "moderately" or "highly" weathered, with not many rock bridges;
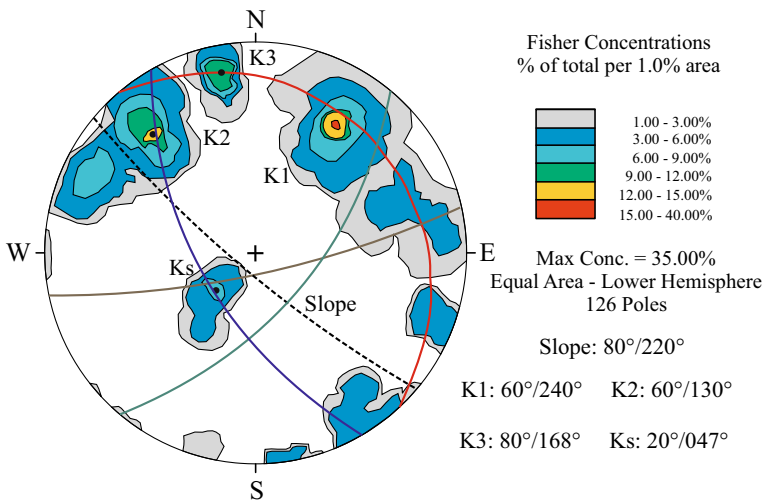

Fig. 3 Stereographic projection of the joint sets affecting the rock mass. Statistical data regarding joint orientations are reported in Table 4

- Usually joint apertures range between "moderately wide" to "wide" (2–15 mm), but also apertures up to 40 mm have been found;
- The block volume (V_b) mostly ranges between 0.32 and 0.37 m^3 with a mean value of about 0.36 m^3 and $\sigma = 0.02$ m^3;
- The roughness, measured by means of the Barton comb (Barton and Choubey 1977) is "smooth, planar" for bedding planes (JRC values 2–6), whereas it is "rough, undulating" (JRC values 6–10) for joints belonging to the other sets.

3 Wave characteristics and longshore energy flux

Even though no quantitative model has yet been proposed in order to evaluate interrelationships between waves, material properties, failure mechanisms and to account for episodic coastal recession of short sea-cliffs (Castedo et al. 2013), wave energy at the cliff base undoubtedly represents an important landslide triggering factor. Consequently, an in-depth study regarding the sea conditions affecting the physiographic unit in which the Agropoli promontory is located was performed (Fig. 4). This coastal stretch is affected by waves mainly incoming from N210° and N285°. The maximum fetch lies between the headings N255° (*Capo Spartivento*, Sardinia) and N240° (*Cap de Garde*, Tunisia) and has a maximum of about 900 nautical miles (Budetta et al. 2008). With reference to the period 1989–2003, the wave characteristics in deep-water have been inferred from data of the *Rete Ondametrica Nazionale* (RON) of the Italian Ministry of Infrastructures and Transports, particularly from the ondameter at Ponza (APAT 2014). The recordings at Ponza are
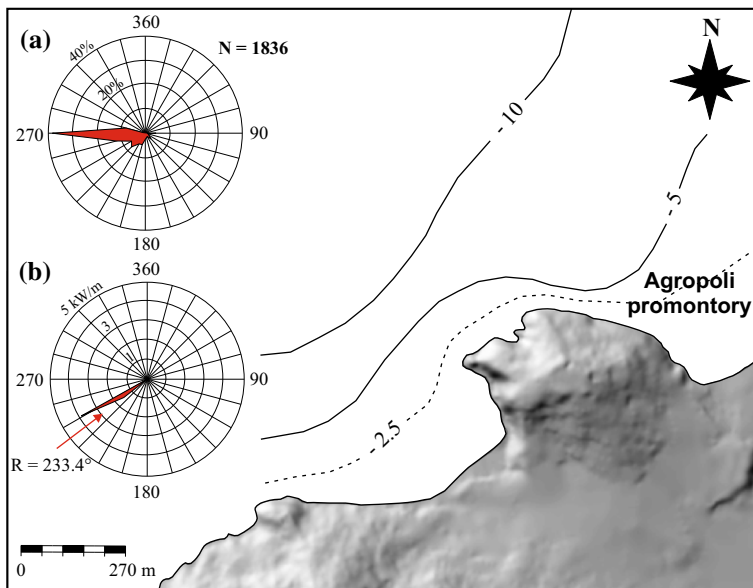

Fig. 4 Bathymetric map of the studied coast. *a* Rose diagram for wave conditions in deep-water (Ponza ondameter) and the relative mean percentage frequencies of the significant wave heights (Hs > 2 m); N = total number of recorded data. *b* Rose diagram for the longshore gross energy flux (isobath −10 m); R = resultant and related direction

considered more valuable for this study, because they refer to an island that is almost unaffected by geographic and orographic factors. Wave data, processed by the RON, made it possible to reconstruct a rose diagram (Fig. 4a) showing that the highest percentage of well-formed waves (of significant height $H_s > 2$ m) occurred from the direction N270°. In the period 1999–2003, the studied coastline was also struck by a large number of sea storms lasting from 1 to 7 days with H_s varying between 2 and 8 m, mainly incoming from the west sector 240°–285° (Fig. 5). Using the wave energy maps developed by means of SWAN ("Simulating Waves Nearshore") model for the whole Italian coastline by Carillo et al. (2012), as well as other unpublished marine data gathered by the competent Regional Agency "Campania sud", referring to erosion phenomena affecting this stretch of regional coast, it was possible to assess the energy amount produced by waves and its direction near the Agropoli promontory. For the period 2001–2010, the mean longshore energy flux affecting the physiographic unit came from a narrow marine sector located between N230° and N240°, having a resultant of about 233.4° (Fig. 4b). The max winter energy amount, reaching about 3.7 kW/m, flows nearly parallel to the coast and mainly affects the windward sector (SW) of the promontory. Considering the local mean direction of the sea-cliff (N310°), this energy flux strikes the cliff toe at approximately a right angle (Fig. 4).

The energy flux that increases during large sea storms favours the erosion process at sea level. During heavy storms, the wave energy strikes the sea-cliff causing the development of a discontinuous notch and the enlargement of joints by rock fragments removal. These phenomena are also promoted by the fair compressive strength of the outcropping rocks and local orientation of some discontinuities near parallel to the predominant wave direction (from the south-west sector). The progressive notch widening causes increasing shear strains along joints, spreading from the notch end towards the cliff top. This occurrence makes local rock collapses easier along K1, K2 and K3 joint sets' intersections (Fig. 6). Another minor triggering factor that can promote these collapses is the insolation weathering. Particularly during the summer period, repeated temperature changes between day and night affecting this area, characterized by a temperate Mediterranean climate, can cause a superficial granular disintegration of the most external film of superficial joints, lowering their shear strength.

4 Geo-mechanical characterization

The physical and mechanical characterization was performed on calcareous marls sampled at different depths along five boreholes (with depth varying between 30 and 50 m) drilled in order to design suitable supports for the sea-cliff protection. Boreholes showed a uniform sequence of calcareous marls (such as those cropping out on the cliff face) affected by variable jointing degree that is reflected by RQD values varying between 65 and 90 %. The widespread presence of buildings in the old town centre caused some boreholes to be drilled at some distance from the cliff top (Fig. 1). Considering the high lithological homogeneity of the rock mass in the whole studied area, the core samples taken are representative. Eight samples were analysed, and their main physical properties are reported in Table 1. By means of qualitative diffractometric tests, it was possible to check that calcite is the predominant component (varying between 65 and 72 %), followed by quartz and muscovite. Based on their petrographic characteristics, these fissile calcareous marls can be technically classified as marlstones.

Deformation and compression strength properties were measured by means of uniaxial compressive strength and point load tests; the variability of results was evaluated on the basis
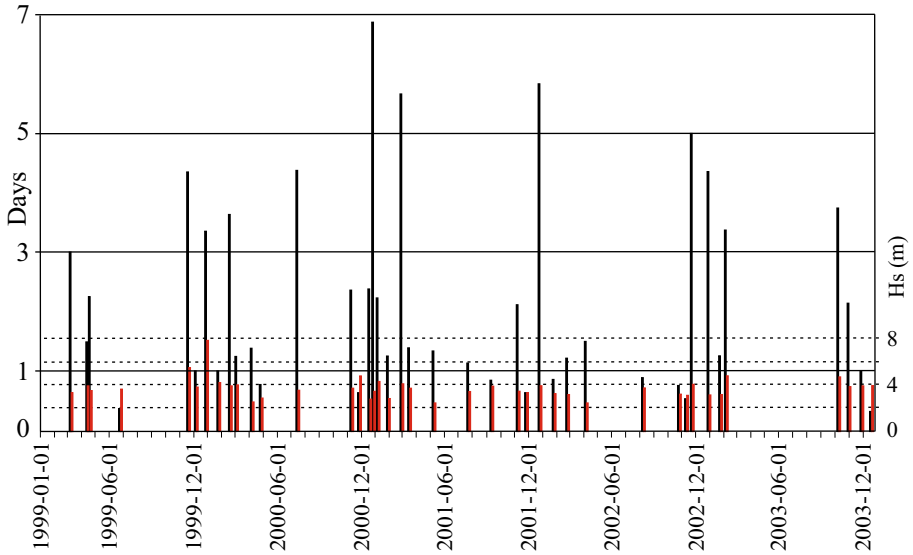
Fig. 5 Duration (*days*) and wave significant heights (*H*s) of sea storms (*red bars*) which struck the studied physiographic unit during the period 1999–2003

Fig. 6 View of the landslide crown of a wedge failure affecting the Agropoli promontory. Several discontinuities near parallel to the predominant wave direction (represented by the *red arrows*) can be also observed

Table 1 Main physical properties of calcareous marls

Property	Min value	Mean value	Max value	Standard deviation
Calcite (%)	65.70	69.31	72.13	2.327
Unit weight (kN/m^3)	25.80	26.13	26.40	0.237
Dry density (kN/m^3)	25.20	25.59	25.90	0.258
Porosity (%)	1.65	1.97	2.48	0.277
Water content (%)	0.63	0.76	0.98	0.133

Table 2 Results of the uniaxial compressive strength and point load tests

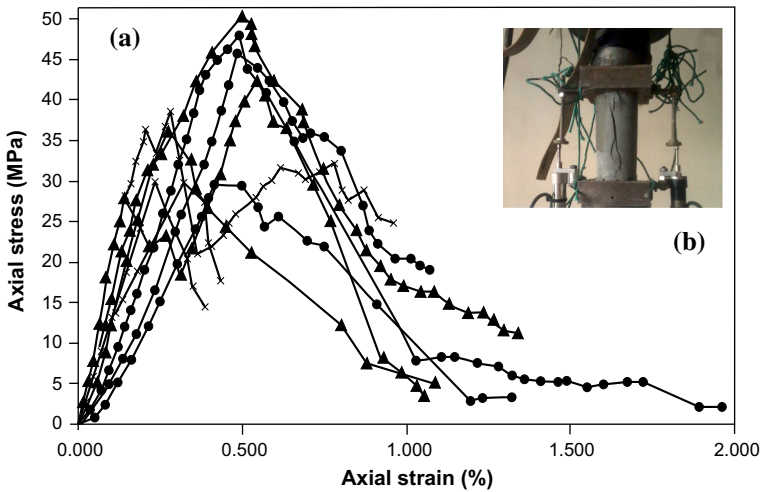| Test	Samples (N)	Min value (MPa)	Mean value (MPa)	Max value (MPa)	Anisotropy index	SD (MPa)	Coeff. var. (%)
Uniaxial compressive strength	9	29.72	38.93	50.73		8.12	20.85
Point load (axial)	24	0.685	1.933	3.116		0.61	31.60
Point load (diametral)	30	0.301	0.640	1.211	3.018	0.29	44.70

Fig. 7 Relationship between axial stress and axial strain for marlstones (*a*); uniaxial compressive test performed on a specimen of marlstone (*b*)

of the standard deviation (SD) and coefficient of variation (C_v) (Table 2). Conforming to ISRM suggested methods (ISRM 2007), uniaxial compressive strength tests were performed on 9 samples with a height-to-diameter ratio of 2.5 and a diameter of about 55 mm. Samples were drilled with the core axis perpendicular to the stratification. Uniaxial Compressive Strength (UCS) values range from about 29 MPa to about 51 MPa with $C_v = 20.85$ %. The diagrams of axial stress versus axial strain (Fig. 7) allowed calculating the Young's tangent moduli at 50 % UCS (*Et*) varying between 9.23 and 21.50 GPa. The finer-textured marlstones gave the highest UCS values with minor axial strains and higher values of moduli.

Point load tests were performed using a digital point load test apparatus carrying out both axial and diametral tests on samples with diameter of 82 mm. According to ISRM (2007), corrections were applied for calculating the size-corrected point load strength index (Is_{50}). Axial and diametral point load tests allowed highlighting a high anisotropy index (Ia) due to stratification (Table 2). Point load values show a higher scattering as compared to UCS results. The correlation between UCS and Is_{50} shows the following linear regression:

$$UCS = 19.5 + 23.9 \ Is_{50} \quad R^2 = 0.82 \tag{1}$$

This regression is in agreement with those reported for similar rock types (such as mudstones and siltstones) by Rusnak and Mark (2000), Tsiambaos and Sabatakakis (2004), and Akram and Bakar (2007).

Conform to the engineering classification based on Et versus UCS by Deere and Miller (1966), the tested samples fall in the D class ("low-strength" rocks). The marlstone envelope extends into the average modulus ratio range (Et/UCS ∼ 350), and its position is considered to be the result of a fair cemented, porous texture and of anisotropy due to bedding planes. When the normal stress increases, deformation is mainly caused by clamping of bedding plane apertures.

The shear strength properties along joint surfaces in marlstones were evaluated by means of the Hoek's shear box. In order to obtain basic (ϕ_b), peak (ϕ_p) and ultimate (ϕ_u) friction angles (Barton 2013), tests were performed on 25 core samples (diameter of about 82 mm) containing unweathered natural or artificial (obtained by sawing and fracturing) discontinuities (Fig. 8). On samples, JRC values were determined both before and after shearing tests by means of the Barton comb. Furthermore, using the Schmidt hammer on joint walls of the tested samples, the joint compressive strength (JCS) values were calculated according to the following formula (Barton and Choubey 1977):

$$\text{Log JCS} = 0.00088\gamma\, r + 1.01 \qquad (2)$$

where γ is the unit weight of the rock and r is the rebound number measured by means of the Schmidt hammer.

Comparing JCS values calculated both after peak (mean JCS = 36.64 MPa) and ultimate shear strength (mean JCS = 29.48 MPa) respectively, a reduction in about 20 % mainly due to disturbance caused by the shearing stress on weak joint walls was estimated.

With reference to smooth, artificial joints obtained by sawing, a mean ϕ_b value of about 35.5° was measured (Table 3; Fig. 8). This agrees well with values obtained on similar rocks by Barla et al. (1986), and more recently by Geertsema (2002). During reversal tests, performed varying the shearing direction and normal stress (σ_n), a small reduction in the shear strength was measured (about 5 %) as well as a drop of ϕ_b when σ_n increased (Fig. 9). ϕ_p values, varying between about 30° and 49°, were calculated with reference to a range of normal stress ($\Delta\sigma_n = 0.2$–0.7 MPa) consistent with that involved in the most
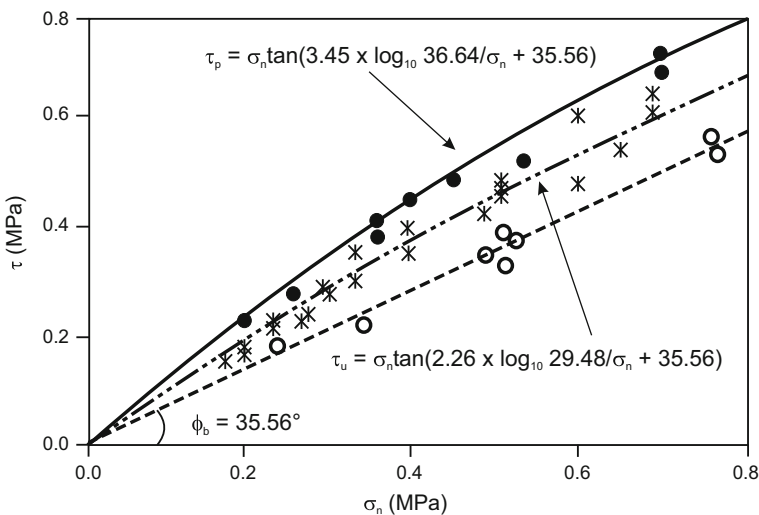

Fig. 8 Nonlinear shear strength criterion according to Barton and Choubey (1977), for tested joints

Table 3 Shear testing results

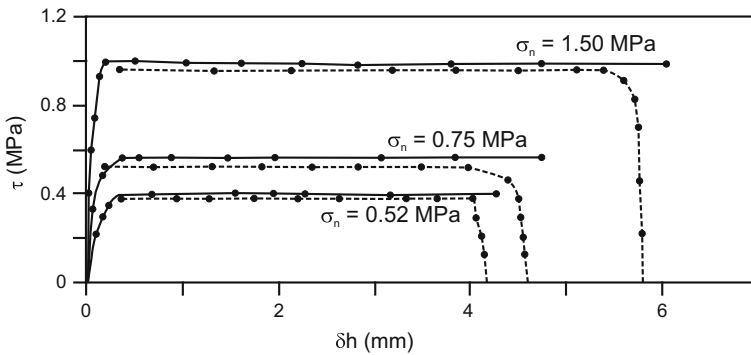|	Data (N)	$\Delta\sigma_n$ (MPa)	Min value (°)	Mean value (°)	Max value (°)	SD (°)
Basic friction angle	14	0.5–2.0	32.47	35.56	39.05	1.97
Peak friction angle	10	0.2–0.7	29.65	42.04	48.81	5.80
Ultimate friction angle	28	0.2–1.0	26.57	39.61	45.56	4.64

Fig. 9 Shear stress–shear displacement plot for an artificial (obtained by sawing) discontinuity

common rock slope stability analysis (Table 3; Fig. 8). During the shear displacement, such range was also adopted with the aim of avoiding the overturning of the upper normal load jack of the box.

Test data were interpolated using the nonlinear regression by Barton and Choubey (1977):

$$\tau = \sigma_n \tan\left[\text{JRC } \log_{10}(\text{JCS}/\sigma_n) + \phi_b\right] \tag{3}$$

JRC was evaluated according to the following formula (Barton and Choubey 1977):

$$\text{JRC} = (\phi_p - \phi_b)/\log_{10}(\text{JCS}/\sigma_n) \tag{4}$$

Regarding ϕ_u, by means of several tests, values ranging between 27° and 45.5° were found, corresponding to normal stress ranging between 0.2 and 1.0 MPa. ϕ_u mean values are higher than those of ϕ_b; moreover, similar to ϕ_b and ϕ_p they decrease when σ_n increases. Passing from the peak to ultimate strength, it must be also noted (Fig. 9) that JRC is gradually lowered due to the damage of asperities during each test. A reduction of about 34.5 % was estimated in JRC values mainly due to the flattening of weak joint asperities at high levels of normal stress. As regards the strength-deformation-dilation trends (Fig. 10), it is interesting to note that dilation occurs only at lower normal stress (0.20–0.25 MPa) and the upper rock block slides along the joint wall by climbing asperities. As normal stress increases, dilation progressively decreases, asperities are sheared and contraction is the predominant deformation behaviour.

The determination of hydraulic properties of the rock mass was done by means of 20 Lugeon water pressure tests (cycles from lower to higher pressure and back) performed in 5 boreholes. As boreholes were located near the slope edge (Fig. 1), the calculated
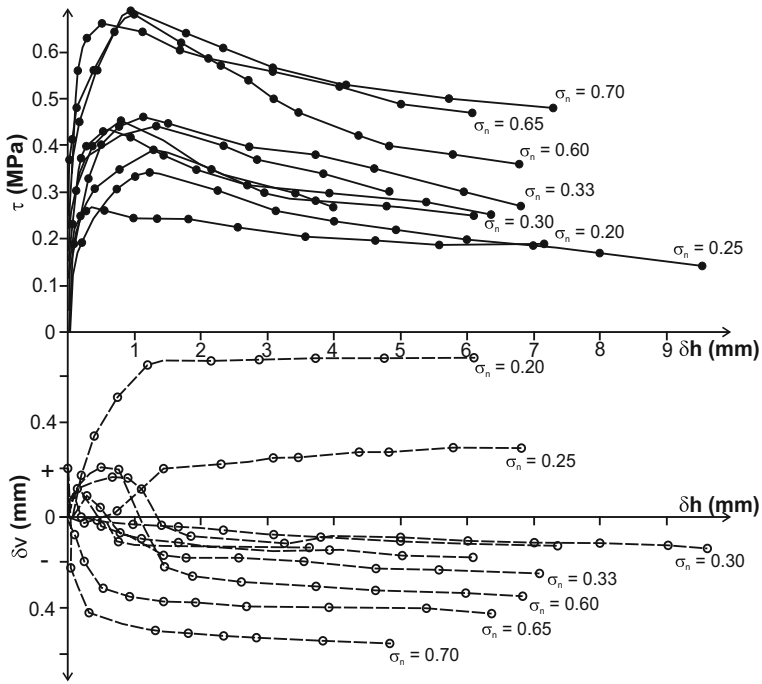
Fig. 10 Strength-deformation-dilatation trends (range of normal stress $\Delta\sigma_n = 0.2$–0.7 MPa) for some tested joints
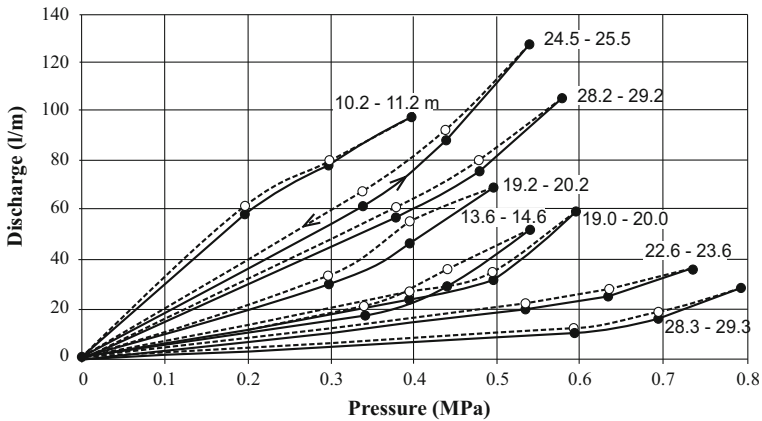

Fig. 11 Results of cyclic water pressure tests conducted from lower to higher pressure and back at different depths in vertical boreholes

permeability coefficients are representative of real hydraulic properties of the outcropping rock mass. The water discharge through discontinuities was measured in uncased borehole portions obtained inserting plug seals about 1 m from the bottom of each drilled borehole. For each test, lasted at least 10 min, during which water pressure and flow rate were

measured to ensure they become constant, five pressure stages were considered to complete a "pressure loop" (Fig. 11). Being borehole orientations almost perpendicular to bedding planes, the gathered data allowed evaluating the hydraulic conductivity of this joint set (Ks) mainly influenced by aperture, infilling, weathering and roughness of discontinuities. Only the first lower pressure step in each pressure loop has been considered meaningful and reflective of the natural groundwater flow conditions, consequently a laminar flow has been assumed for the tested joint set. As can be seen from Fig. 13, at higher water pressures ($p > 0.4$–0.5 MPa) turbulent flow conditions begin.

The permeability coefficient (K) expressed in m/s has been calculated from the Hvorslev's (1951) general equation as:

$$K = Q/(F\,h_r) \tag{5}$$

where Q is the flow rate (m^3/s), F is the shape factor (m), and h_r is the real hydraulic head (m), taking account of the charge loss along the pipeline and of the vertical distance between the pressure gauge and the test chamber.

The shape factor F depends on the shape of the test chamber and the flow directions and is given by Maasland and Kirkham (1959):

$$F = \frac{3\pi \cdot L}{\log_e\left[\frac{1.5 \cdot L}{D} + \sqrt{1 + \left(\frac{1.5 \cdot L}{D}\right)^2}\right]} \tag{6}$$

where L is the length of the test chamber (1 m) and D is the diameter of the hole (0.101 m).

The whole range of K values varies between 3.01×10^{-5} and 5.61×10^{-7} m/s, and permeability values generally tend to lower with depth (Fig. 12). This is due to the

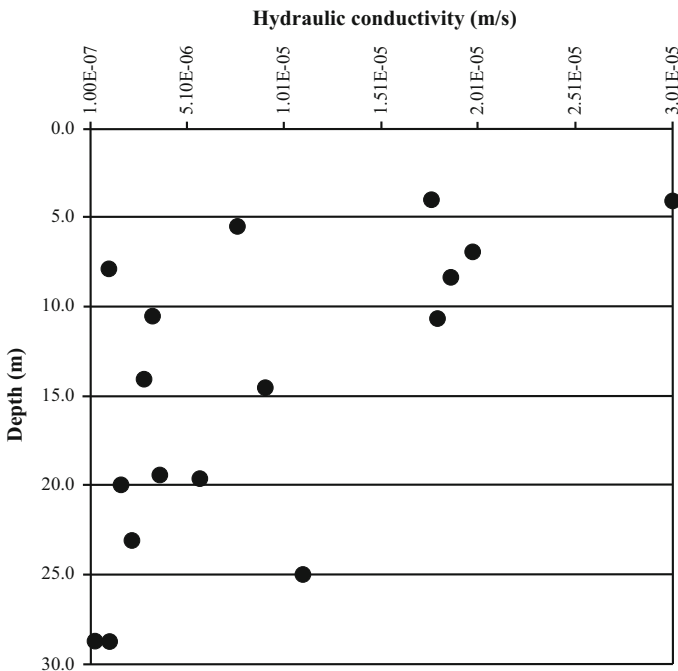
Fig. 12 Hydraulic conductivities versus depth for the Ks joint set

progressive reduction in joint apertures and weathering with depth. Nevertheless, it is worth observing that, caused by a local wider spacing of marlstone strata and lower jointing of the rock mass (mainly between 5 and 15 m), K can attain low values also at minor depths. This occurrence favours a more ready groundwater saturation of discontinuities belonging to K1, K2 and K3 joint sets which are almost orthogonal to stratification. Consequently, critical heights of water promoting instability, during heavy rainfalls, can occur more easily in these joints.

5 Wedge failure stability analysis

In order to evaluate the sea-cliff stability, a geo-mechanical analysis was performed using the limit-equilibrium method for the safety factor (SF) calculation of possible wedge failures. The stability analysis was performed using the suggested approach by Hoek and Bray (1981) implemented in SWEDGE version 5.0 (Rocscience 2013), a software that evaluates the stability of surface wedges in rock slopes. The adopted wedge models are based on the presence of a tension crack, and consider four sliding modes: sliding along the intersection line (no contact on planes), sliding on plane 1, sliding on plane 2, sliding on both planes. As the initial failure process involves the peak shear strength along joints, ϕ_p values were used. Both deterministic and probabilistic analyses were performed considering dry and partially saturated joint conditions, respectively. In order to consider the water seepage during heavy rainfalls, a critical height of water in joints that causes the achievement of the limit-equilibrium condition (SF = 1) was also assumed. In fact, local marlstone strata affected by a lower permeability promote the groundwater storage in tectonic discontinuities belonging to joint sets K1, K2 and K3.

According to Park and West (2001), the probabilistic procedure was developed in two steps, the first examining kinematic instability of wedges defined by joint set intersections, in order to assess whether there are potentially unstable geometric conditions. Afterwards, where the kinematic analysis indicates that this condition exists, the kinetic instability is assessed by the limit-equilibrium method. The kinematic analysis was accomplished using stereographic projections of joint set systems (K1, K2, K3 and Ks), whereas the kinetic instability analysis was performed by means of the Monte Carlo simulation (Grenon and Hadjigeorgiou 2008; Mat Radhi et al. 2008). Joint orientations and friction angles were considered as probabilistic parameters adopting their mean values (M) and standard deviations (σ). Therefore, data uncertainty must be taken into account because scattering in measured and tested data makes mean values poorly significant. Conversely, slope and tension crack orientations, as well as the wedge height, apparent rock density, and height of the static water filling joints were considered to be known.

The overall probability of slope failure (P_f) was evaluated as a conditional probability. That is, based on a number of iterations, if it is possible to assess that joint sets' intersections form wedges which can kinematically move respect to the slope face with a probability (P_{km}) different from zero, then it will be:

$$P_f = P_{km} \times P_{kn} \tag{7}$$

where P_{kn} is the probability of kinetic instability (Einstein 1996).

P_{km} is defined as the ratio between the number of iterations whose result correspond to kinematic instability (N_u) and the total number of iterations (N_T), whereas P_{kn} is given by the ratio between the number of iterations in which a wedge has a factor of safety less than

one (N_f) and N_u. This is because the kinetic analysis is performed only when the block is kinematically unstable (Park and West 2001; Park et al. 2005).

In order to evaluate the kinematic instability, possible intersections between discontinuities belonging to joint set systems, K1, K2, K3 and Ks, were analysed and wedges whose lines of intersection can intersect the slope face, at different angles, were identified. For the whole cliff face, a single mean orientation was considered (dip/dip direction 80°/220°), and no attention was given to the orientation scattering that affects joint sets. This is because, according to the adopted probabilistic procedure, even though the mean orientation of joint sets could yield a kinematically stable condition it is possible that variable orientations of some intersections between discontinuities belonging to the above-mentioned joint sets have the possibility of kinetic instability.

The kinetic instability was evaluated by means of the approach suggested by Hoek and Bray (1981) and using the "probabilistic" option in SWEDGE. As mentioned previously, P_{kn} was calculated by the ratio between N_f and N_u, being N_f the number of failing wedges (SF < 1). In order to compare P_f with SF of all individual kinematically possible failures, in SWEDGE all random variables were replaced by mean values of respective distributions. Kinetic analysis required input data such as the slope geometry, unit weight of rock, joint orientations, peak shear strength of joint surfaces and the critical height of water in joints (Table 4). From these input data distributions, the Monte Carlo sampling technique was implemented re-running SWEDGE in accordance with the probabilistic approach, and for each analysis was assumed $N_T = 10,000$. Probabilities of the four possible sliding modes were evaluated.

Table 5 shows results of deterministic and probabilistic analyses for all possible joint set combinations. For only two joint set combinations (K2–Ks and K3–Ks), it is possible to note that they are stable (from a deterministic point of view) and have zero probability of kinematic instability. It is worth observing that "stable" intersections between joint sets refer to wedges whose lines of intersection dip into the rock face favouring a better stability. Other two stable joint combinations (K1–Ks and K2–K3) show kinematic probabilities ranging between 17 and 4.2 %. This is because there is a wide scatter of joint orientations with respect to the mean values, which make some wedge failure possible. However, based on kinetic analysis, there is not failure probability for these wedges. By contrast, the joint set combination K1–K2 shows the highest probability value of kinematic instability (95.7 %), whereas the result of the kinetic analysis shows a 16 % possibility of sliding on both planes and only 6.1 % possibility of a sliding mode in contact on plane 1 (according to the dry condition). Consequently, P_f is 21.1 % for this joint set combination. It is worth observing that even though this combination is a kinematically unstable condition, the deterministic SF value was calculated to be 1.29, for a sliding mode with contact on both planes. Consequently, based on the deterministic analysis in dry conditions, wedges arising from K1 and K2 intersections should be quite stable with respect to the slope face. On the contrary, assuming a critical height of water in joints of about 0.40 m, wedges achieve the limit-equilibrium condition (SF = 1) and P_f is twice the value of dry condition.

Finally, the combination K1–K3 has SF = 0.52 (considering a dry condition and sliding mode on plane 1) and also shows a high kinematic instability (85.1 %). As the kinetic analysis also shows high probability values of sliding (for both the above-mentioned sliding modes 2 and 4), P_f for this combination is very high (73.4 %). Assuming, for every joint, a height of static water equal to 0.40 m, then P_f reaches a value close to 84 %.

On the basis of wedge geometries and trace lengths of discontinuities on the slope face, SWEDGE also allowed evaluating the average volume that could be generated by joint set

Table 4 Input values for probabilistic and deterministic analysis

	Slope face orientation (°)	Upper slope face orientation (°)	Height of the slope (m)	Unit weight of rocks (kN/m³)
(a) Input for cliff geometry	80/220	12/220	35	26.0

Set no.	K1	K2	K3	Ks
(b) Input for joint properties				
Mean orientation (°)	60/240	60/130	80/168	20/047
Standard deviation (°)	8.5/14.9	8.5/13.0	4.3/14.0	6.3/20.4
Coefficient of variation (%)	14.2/6.2	14.2/10.0	5.3/8.3	31.5/43.4
Mean friction angle (°)	42	42	42	42
Standard deviation (°)	5.80	5.80	5.80	5.80
Critical height of water in the joints (m)	0.40	0.40	0.40	0.40

Table 5 Results of wedge failure according to deterministic and probabilistic analysis

Set no. 1	Set no. 2	Safety factor (deterministic)	Probability of failure					Overall probability of failure	Average volume of possible wedge (m^3)
			Kinematic	No contact	Plane 1	Plane 2	Both planes		
K1	K2	SF$_4$ = 1.29/1.00	0.957	0	0.061/0.120	0	0.160/0.320	0.211/0.421	28.07
K1	K3	SF$_2$ = 0.52	0.851	0	0.473/0.530	0	0.390/0.462	0.734/0.844	10.68
K1	Ks	Stable	0.170	0	0	0	0	0	0
K2	K3	Stable	0.042	0	0	0	0	0	0
K2	Ks	Stable	0	0	0	0	0	0	0
K3	Ks	Stable	0	0	0	0	0	0	0

For any joint set combination, are reported SF and Pf values for both the dry condition and assuming a critical height of water (0.40 m) in joints, respectively. Values also refer to possible four sliding modes (no contact on planes, sliding on joint 1 or 2 alternatively and sliding on both planes)

combinations. A difference between average volumes of possible wedges formed by K1–K2 and K1–K3 can be seen (Table 5). However, considering the overall failure probability and correlated SF values affecting the above-mentioned combinations, smaller wedge failures, which could happen more frequently, can be expected, generating by K1–K3 intersections (about 11 m^3). Unfortunately, there is not landslide inventory data that can validate results of the employed software.

6 Zonation of wedge failure probability

On the basis of joint set data surveyed in the four homogeneous geo-structural sectors (Fig. 2) and results of the probabilistic analysis, a tentative zonation of areas affected by variable wedge failure probabilities was proposed (Fig. 13). The zonation model was prepared by depicting, on a simplified photogrammetric map of the whole sea-cliff, areas in which crop out the joint set combinations K1–K2 and K1–K3, individually and/or jointly considered. Failure probability values calculated for each joint set combination (considering both the dry condition and the water seepage into joints) have been assigned to all possible wedge geometries caused by the intersection of the detected joint systems K1, K2 and K3, with respect to the cliff face orientation.

Geo-structural sectors 1, 3 and 4, where joint set combinations K1–K2 and K1–K3 are individually present, can be considered as zones affected by "high wedge failure probability". In these areas, on the basis of the probabilistic analysis, it was possible to assess that the joint set combination K1–K3 shows failure probabilities (P_f varying between 73.4 and 84.4 %) higher than those characterizing the joint set combination K1–K2. Where the above-mentioned combinations simultaneously affect the rock mass (particularly in the sector 4), the wedge failure probability resulting from interaction of two joint set combinations can be considered as "very high". Even though only the most south-eastern area of this sector shows this condition, the slope height (about 55 m) and its irregular shape
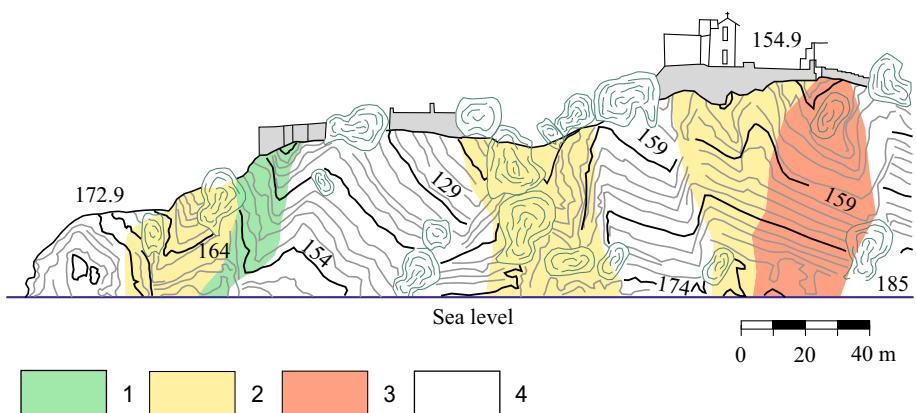

Fig. 13 Tentative wedge hazard zonation of the sea-cliff. *1* Cliff area mainly affected by the joint set combination K1–K2 having P_f values varying between 21 and 42 %; *2* cliff area mainly affected by the joint set combination K1–K3 having P_f values varying between 73 and 84 %; *3* cliff area mainly affected by the presence of both hazardous joint set combinations; *4* cliff area affected by "stable" joint set combinations or with combinations having zero probability of kinematic and/or kinetic instability

could favour higher run-out distances of falling and rebounding blocks at the cliff base, where a sandy beach exploited for bathing purposes is located (Fig. 1).

It should be noted that sometimes geo-structural sectors of the sea-cliff (particularly the sector 2) are characterized by "stable" (from a deterministic point of view) joint set combinations or with combinations having zero probability of kinematic and/or kinetic instability (Table 5). Nevertheless, during large sea storms the assailing force of waves at the cliff base can cause the rock block removal, creating favourable conditions for failures of previously restrained wedges. In such a way, retrogressive landslides can happen. Consequently, also these areas are affected by a high landslide hazard level (Fig. 13).

7 Discussion and conclusions

In the international literature, there are several investigations concerning the landslide hazard assessment of rocky coasts. These studies take into account long coastal stretches evaluating hazard on the basis of the geomorphological instability, lithological layout, wave climate and erosion rates. Usually, erosion rates are estimated using historical aerial photographs and maps or comparing cliff edges digitized from historical maps with recent cliff edges, generally interpreted from LIDAR surveys or other topographical methods. Then, landslide hazard can be evaluated considering, for the future, the current cliff retreat rate and applying qualitative or quantitative methods (Hapke et al. 2007).

Where there is a lack of these data, and collapses of short sea-cliffs are episodic and discontinuous in time and space, it is preferable to use probabilistic approaches based on geo-structural and geo-mechanical data, that is, if adequate data are available, as in the studied case history. The above-described approach was applied along the coastal stretch of Southern Italy, where the Agropoli promontory is located. It showed that the sea-cliff areas affected by K1–K3 and K1–K2 joint intersections, individually and/or jointly considered, have high wedge failure probabilities. Also wave motion could make the sea-cliff stability conditions worse. During heavy sea storms, waves erode the cliff toe, undercutting and over-steepening it. This may destabilize blocks bounded by "stable" intersections and promote retrogressive landslides along the overlying slope. At the cliff base, the notch development and its temporal widening are promoted by the low strength of marlstones. With regard to this, the geo-mechanical study demonstrates that marlstones are characterized by a compressive strength varying between 29 and 51 MPa with an average modulus ratio falling in the D class ("low-strength" rocks), according to Deere and Miller classification. This is caused by their fair diagenesis degree, porous texture and high anisotropy. Also karst phenomena and corrosion, due to sea spray, worsen the stability favouring the enlargement of joint apertures.

The wedge failure probability affecting the sea-cliff is strongly influenced by the geo-structural and geo-mechanical layout of the rock mass and subordinately the assailing force of waves. The random properties of orientation and shear strength of joints have an important effect in the safety factor calculation. As the deterministic approach does not take into account the variability of these parameters and can provide simplified and misleading results, the simultaneous analysis of kinematic and kinetic conditions which can provide a better evaluation of the overall failure probability is preferable.

References

Agenzia per la protezione dell'ambiente ed i servizi tecnici-APAT (2014) Atlante delle coste. "Il moto ondoso a largo delle coste italiane". http://www.isprambiente.gov.it/files/atlante-coste/. Accessed 20 April 2014

Akram M, Bakar MZA (2007) Correlation between uniaxial compressive strength and point load index for Salt-Range rocks. Pak J Eng Appl Sci 1:1–8

Andriani GF, Walsh N (2007) Rocky coast geomorphology and erosional processes: a case study along the Murgia coastline south of Bari, Apulia- SE Italy. Geomorphology 87(3):224–238

Antonioli F, Silenzi S (2007) Variazioni relative del livello del mare e vulnerabilità delle pianure costiere italiane. Quaderni Soc Geol It 2: 2–23. http://www.socgeol.it/317/quaderni.html

Ashton AD, Walkden MJA, Dickson ME (2011) Equilibrium responses of cliffed coasts to changes in the rate of sea level rise. Mar Geol 284:217–229

Barla G, Forlati F, Scavia C (1986) Caratteristiche di resistenza al taglio di discontinuità naturali in roccia. Riv It Geotecnica 20(4):219–235

Barton N (2013) Shear strength criteria for rock, rock joints, rockfill and rock masses: problems and some solutions. J Rock Mech Geotech Eng 5(4):249–261

Barton N, Choubey V (1977) The shear strength of rock joints in theory and practice. Rock Mech 12:1–54

Bonardi G, Ciarcia S, Di Nocera S, Matano F, Sgrosso I, Torre M (2009) Carta delle principali unità cinematiche dell'Appennino meridionale. Nota illustrative. It J Geosci 128(1):47–60

Budetta P (2011) Stability of an undercut sea-cliff along a Cilento coastal stretch (Campania, Southern Italy) Nat Hazards 56:233–250. doi 10.1007/s11069-010-9565-y

Budetta P, Nappi M (2011) Heterogeneous rock mass classification by means of the geological strength index: the San Mauro formation (Cilento, Italy). Bull Eng Geol Environ 70:585–593. doi:10.1007/s10064-011-0351-1

Budetta P, Galietta G, Santo A (2000) A methodology for the study of the relation between coastal erosion and the mechanical strength of soils and rock masses. Eng Geol 56:243–256

Budetta P, Santo A, Vivenzio F (2008) Landslide hazard mapping along the coastline of the Cilento region (Italy) by means of a GIS-based parameter rating approach. Geomorphology 94(3–4):340–352

Carillo A, Bargagli A, Caiaffa E, Iacono R, Sannino G (2012) Stima del potenziale energetico associato al moto ondoso in regioni campione della costa italiana. Rapporto tecnico. ENEA Report RdS-2012-170, p 30. http://openarchive.enea.it/handle/10840/4525. Accessed 20 April 2014

Castedo R, Fernández M, Trenhaile AS, Paredes C (2013) Modeling cyclic recession of cohesive clay coasts: effects of wave erosion and bluff stability. Marine Geol 335:162–176. doi: 10.1016/j.margeo.2012.11.001

Church JA, White NJ (2006) A 20th century acceleration in global sea-level rise. Geophys Res Lett 33(L01602):1–4. doi:10.1029/2005GL024826

De Vita P, Cevasco A, Cavallo C (2012) Detailed rock failure susceptibility mapping in steep rocky coasts by means of non-contact geo-structural surveys: the case study of the Tigullio Gulf (Eastern Liguria, Northern Italy). Nat Hazards Earth Syst Sci 12:867–880. doi:10.5194/nhess-12-867-2012

Deere DU, Miller RP (1966) Engineering classification and index properties for intact rocks. Technical report no. AFWL-TR-65-116. University of Illinois, Urbana, p 229

Di Crescenzo G, Santo A (2007) High-resolution mapping of rock fall instability through the integration of photogrammetric, geomorphological and engineering-geological surveys. Quatern Int 171–172:118–130

Dubois RN (2002) How does a barrier shoreface respond to a sea-level rise? J Coast Res 18(2):III–V

Einstein HH (1996) Risk and risk analysis in rock engineering. Tunn Undergr Space Technol 11(2):141–155

Geertsema AJ (2002) The shear strength of planar joints in mudstone. Int J Rock Mech Min Sci 39:1045–1049

Grenon M, Hadjigeorgiou J (2008) A design methodology for rock slopes susceptible to wedge failure using fracture system modelling. Eng Geol 96:78–93

Hall AM, Hansom JD, Jarvis J (2008) Patterns and rates of erosion produced by high energy wave processes on hard rock headlands: the Grind of the Navir, Shetland, Scotland. Mar Geol 248:28–46. doi:10.1016/j.margeo.2007.10.007

Hapke C, Reid D, Borrelli M (2007) The national assessment of shoreline change: a GIS compilation of vector cliff edges and associated cliff erosion data for the California coast. US Geol Survey, open-file report 2007-1112

Hoek E, Bray JW (1981) Rock slope engineering. The Institution of Mining and Metallurgy, London

Hvorslev MJ (1951) Time lag and soil permeability in groundwater observations. US Army corps of engineers waterways experiment station, Vicksburg, Mississippi. Bull. 36

Intergovernmental Panel on Climate Change-IPCC (2007) Synthesis report, contribution of working group I to the fourth assessment report of the intergovernmental panel on climate change, 2007. http://www.ipcc.ch/publications_and_data/ar4/wg1/en/contents.html. Accessed 20 April 2014

International Society of Rock Mechanics—ISRM (2007) The complete ISRM suggested methods for rock characterization, testing and monitoring: 1974–2006. In: Ulusay R, Hudson JA (eds) Suggested methods prepared by the commission on testing methods. International society for rock mechanics, compilation arranged by the ISRM Turkish National Group, Ankara, Turkey

Kogure T, Aoki H, Maekado A, Hirose T, Matsukura Y (2006) Effect of the development of notches and tension cracks on instability of limestone coastal cliffs in the Ryukyus, Japan. Geomorphology 80(3–4):236–244

Maasland M, Kirkham D (1959) Measurement of permeability of triaxially anisotropic soils. Proc Am Soc Chem Eng 85(SH 3 No. 2063):25–34

Marques FMSF, Matildes R, Redweik P (2013) Sea cliff instability susceptibility at regional scale: a statistically based assessment in the southern Algarve, Portugal. Nat Hazards Earth Syst Sci 13:3185–3203. doi:10.5194/nhess-13-3185-2013

Martino S, Mazzanti P (2013) Analysis of sea cliff slope stability integrating traditional geo-mechanical surveys and remote sensing. Nat Hazards Earth Syst Sci Discuss 1:3689–3734. doi:10.5194/nhessd-1-3689-2013

Mat Radhi MS, Mohd Pauzi NI, Omar H (2008) Probabilistic approach of rock slope stability analysis using Monte Carlo simulation. In: Al-Mattarneh H, Kamaruddin I, Resheidat M (eds) Advanced research in transportation and geotechnical engineering. Proceedings of the international conference on construction and building technology 2008, Kuala Lumpur, Malaysia, E(37), pp 449–469. ISBN 967-958-161-6

Naylor LA, Stephenson WJ (2010) On the role of discontinuities in mediating shore platform erosion. Geomorphology 114:89–100. doi:10.1016/j.geomorph.2008.12.024

Palmström A (2005) Measurements and correlations between block size and Rock Quality Designation (RQD). Tunn Undergr Sp Tech 20(4):362–377

Park H, West TR (2001) Development of a probabilistic approach for rock wedge failure. Eng Geol 59:233–251

Park H, West TR, Woo I (2005) Probabilistic analysis of rock slope stability and random properties of discontinuity parameters, interstate highway 40, Western North Carolina, USA. Eng Geol 79:230–250

Paronuzzi P (2010) Flexural failure phenomena affecting continental Pleistocene deposits along coastal cliffs (Croatia). Ital J Eng Geol Environ 1:93–106. doi:10.4408/IJEGE.2010-01.0-07

Rocscience inc (2013) SWEDGE-3D surface wedge analysis for slopes (version 5.0). Toronto, Ontario, Canada. http://www.rocscience.com

Rusnak J, Mark C (2000) Using the point load test to determine the uniaxial compressive strength of Coal Measure rock. In: Peng SS, Mark C (eds) Proceedings of the 19th international conference on ground control in mining. West Virginia University, Morgantown, pp 362–371

Sunamura T (1992) Geomorphology of rocky coasts. Wiley, Chichester

Trenhaile AS (2002) Rock coasts, with particular emphasis on shore platforms. Geomorphology 48:7–22

Tsiambaos G, Sabatakakis N (2004) Considerations on strength of intact sedimentary rocks. Eng Geol 72:261–273